must exist to permit the molecules to be situated in such a way that they are not screened by being "buried" in the top metal film. Other explanations, of course, are also possible. The occurrence of molecular spectra in Y-(Y oxide)-metal diodes could not be tested.

ACKNOWLEDGMENTS

The authors wish to thank R. M. Ager and E. B. Schermer for technical assistance in the tunneling experiments, and J. L. Parsons for making the reflectivity measurements.

[1]R. C. Jaklevic and J. Lambe, Phys. Rev. Letters 17, 1139 (1966); J. Lambe and R. C. Jaklevic, Phys. Rev. 165, 821 (1968).
[2]A. L. Geiger, B. S. Chandrasekhar, and J. G. Adler, Phys. Rev. Letters 188, 1130 (1969).
[3]I. Giaever and H. R. Zeller, Phys. Rev. Letters 21, 1385 (1968).
[4]J. M. Rowell and W. L. McMillan, Bull. Am. Phys. Soc. 12, 77 (1967).
[5]J. G. Adler, Solid State Commun. 7, 1635 (1969).
[6]R. C. Jaklevic and J. Lambe, Bull. Am. Phys. Soc. 14, 43 (1969); J. M. Rowell, W. L. McMillan, and W. L. Feldman, Phys. Rev. 180, 658 (1969).
[7]J. A. Appelbaum and W. F. Brinkman (unpublished); A. D. Brailsford and L. C. Davis (unpublished).
[8]L. Y. L. Shen and J. M. Rowell, Phys. Rev. 165, 566 (1968).
[9]A similar observation has recently been reported by L. Y. L. Shen, J. Appl. Phys. 40, 5171 (1969).
[10]A. A. Milgram and Chih-Shun Lee, J. Appl. Phys. 39, 2851 (1968).
[11]See, for example, *Sadtler Standard Spectra* (Sadtler Research Laboratories, Philadelphia, Pa., 1900).
[12]K. A. Wickersheim and R. A. Lefever, J. Opt. Soc. Am. 51, 1147 (1961); N. J. McDevitt and A. D. Davidson, *ibid.* 56, 636 (1966).
[13]D. R. Renneke and D. W. Lynch, Phys. Rev. 138, A530 (1965); R. Marshall, S. S. Mitra, P. J. Gielisse, J. N. Plendl, and L. C. Mansur, J. Chem. Phys. 43, 2893 (1965).
[14]O. Kubaschewski and B. E. Hopkins, *Oxidation of Metals and Alloys* (Butterworths, London, 1962).
[15]H. B. Möller and A. R. Mackintosh, *Inelastic Scattering of Neutrons in Solids and Liquids* (International Atomic Energy Agency, Vienna, 1965), Vol. 1, p. 95; J. L. Feldman, Phys. Rev. (to be published).
[16]M. Mikkor and W. C. Vassell (unpublished).

PHYSICAL REVIEW B VOLUME 2, NUMBER 4 15 AUGUST 1970

Measurement of the Anisotropic Resistivity Tensor of Silver Using Heliconlike Waves*

D. V. Giovanielli† and J. R. Merrill
Department of Physics and Astronomy, Dartmouth College, Hanover, New Hampshire 03755
(Received 18 March 1970)

Standing-wave resonances of heliconlike waves have been used to measure resistivity tensor elements R_{ij} in silver single crystals. Flat-plate samples were used. Data were taken for ±12° regions near the major directions [100], [111], [110], and [211]. Curves are presented of the variation of the R_{ij} elements with field direction. Data are also presented as functions of field strength with the field direction fixed along major directions. Reversing the field allowed the separation of terms even and odd in field. These data represent a more complete study of resistivity tensor elements in silver for field directions near major axes than has previously been available.

I. INTRODUCTION

Electromagnetic heliconlike waves have been used to measure the elements of the anisotropic resistivity tensor of silver as functions of crystallographic direction near the principal axes. The results are a more complete study of resistivity tensor elements for directions near principal axes than has previously been available. dc measurements of galvanomagnetic properties of metals have been used for some years to help determine Fermi-surface topology.[1] dc measurements of the transverse magnetoresistance[2] indicate that the silver Fermi surface makes contact with the Brillouin-zone boundary.

In the present ac experiments, flat-plate samples were used whose normals lay along the major crystallographic directions. The propagation direction for the waves was along the plate normal. The theory for helicons in this geometry is well

known.[3] Standing waves are set up whenever an integral number of half-wavelengths just fit into the sample thickness. The resulting resonance in wave amplitude exhibits a characteristic Lorentzian line shape as a function of frequency. Three measurable parameters are sufficient to describe the resonance: the resonant amplitude A; the quality factor Q; and the resonant frequency f_r. In the present experiments the magnetic field direction was tipped up to $\pm 12^\circ$ with respect to the plate normal. In this case an additional multiplicative factor occurs in the theory. This factor is of order $\cos\theta$, where θ is the angle between the field and the propagation vector. For $\theta \leqq 12^\circ$ this factor can be set equal to unity.

Previous helicon anisotropy measurements made on silver[4] used cylindrical samples with the static field $\vec{B}_0$ and propagation vector $\vec{k}$ perpendicular to the cylinder axis. This geometry is experimentally very appealing, but involves a boundary-value problem which is not understood.

In the flat-plate geometry the resonance parameters can be directly related to the elements of the resistivity tensor R_{ij}.[3] For an infinite flat plate, anisotropic medium with the static field $\vec{B}_0$ in the z direction it is found that

$$A \propto R_{xy}/(R_{xx}+R_{yy}) \quad , \tag{1a}$$

$$Q = (R_{xx}R_{yy} - R_{xy}R_{yx})^{1/2}/(R_{xx}+R_{yy}) \quad , \tag{1b}$$

$$f_r = (\pi/2\mu_0 d^2)(R_{xx}R_{yy} - R_{xy}R_{yx})^{1/2} \quad . \tag{1c}$$

All units are mks. One can invert these measurable parameters to get the R_{ij} elements transverse to $\vec{B}_0$ as functions of crystallographic direction. One can also obtain R_{ij} elements as functions of magnetic field for a specific field direction.

II. EXPERIMENTAL ARRANGEMENT

The instrumentation used in this experiment is shown schematically in Fig. 1. Similar instrumentation used to measure helicon resonances has been reported earlier.[4-6] The oscillator produced two audio-frequency signals, one at a chosen phase with respect to the other. One signal was used to excite a drive coil D through a power amplifier; the other oscillator signal was attached to the horizontal amplifier of an oscilloscope. The drive coil and the pickup coil P were free-standing coils of rectangular cross section. Their natural resonant frequencies (~ 60 kHz) were well above the observed helicon frequencies. The sample plates fit snugly into the pickup coil. A coating of petroleum jelly held the samples rigidly in place at low temperatures. The pickup coil itself fit snugly into the drive coil and was also cemented in place with petroleum jelly. The axes of the two coils were carefully aligned to be perpendicular to each other, minimizing direct induction pickup.

The coil-sample assembly was inserted into a 30-kG superconducting solenoid. The coils were mounted so that the sample could then be tipped up to $\pm 12^\circ$ with respect to the static field while keeping the drive field perpendicular to $\vec{B}_0$. The drive coil was cemented to a small table hinged at one end and mounted in a micarta former. The axis of the drive coil was parallel to the rotation axis of the table and perpendicular to $\vec{B}_0$. A beryllium copper spring held the table against a threaded brass rod. Turning the rod tipped the coils and sample in the large field $\vec{B}_0$. The drive field remained perpendicular to $\vec{B}_0$ and parallel to the sample surface. Phosphor bronze springs attached to the micarta former held the experiment firmly in the superconducting solenoid, avoiding low-frequency mechanical resonances.[5]

The entire assembly was placed in a liquid-helium cryostat. The sample tipping mechanism was operated from outside the cryostat. Angular resolution of better than 0.1° was possible. A dc voltage source attached to the tipping mechanism provided a voltage proportional to the tip angle. This voltage, together with a voltage proportional to the driving frequency, was read by a data-acquisition system. This system converted the analog data into digital information and produced a punched paper tape which could be read directly by a digital computer.

The pickup signal was attached to the vertical amplifier of the oscilloscope and through an amplifier to an ac voltmeter. The voltmeter produced a dc output proportional to the helicon amplitude. This voltage was also read by the data-acquisition system.

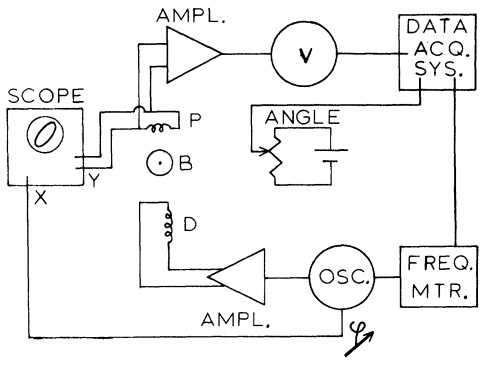

FIG. 1. Schematic diagram of instrumentation. P and D are the rectangular cross-section pickup and drive coils, respectively. The data-acquisition system reads the helicon amplitude and frequency, and the angle of the field relative to the silver crystal.

At resonance the phase of the helicon is 90° with respect to the driving signal. After setting the variable phase output of the oscillator to 90°, the frequency could be adjusted to close the Lissajous ellipse on the oscilloscope. The data-acquisition system was then triggered to record angle, amplitude, and frequency. The same data were taken for the upper and lower half-power points of the resonance. These points are ±45° out of phase with the resonance. The angle of the crystal relative to the field was then changed, and the procedure repeated. The data yielded the parameters A, Q, and f_r directly as functions of the crystallographic orientation of the field $\vec{B}_0$. The measurements were repeated with the field reversed. Terms in the R_{ij} elements even and odd in magnetic field could then be obtained. Alternatively, the sample could be fixed in the field in a specific orientation and the data taken as a function of field strength.

III. RESULTS

Results are reported for four silver samples whose normals were along the [100], [110], [111], and [211] crystallographic axes. Each sample was approximately 1 mm thick with face dimensions of about 15 mm. The ratio of side length to thickness was sufficiently large to allow the use of the helicon theory developed for an infinite flat plate.[6] Table I lists pertinent sample information for the four samples investigated. All samples were spark cut from the same single-crystal rod. Data were taken as a function of orientation in the magnetic field with a field of 30 kG, and as functions of field strength along the four major directions.

Figures 2–4 show the variation with field direction of the helicon resonance parameters for the samples whose normals were along the [111], [100], and [211] axes, respectively. The origin of the angle scale was chosen to be at the position of the major direction as determined by the helicon resonant amplitude. In all cases previous x-ray determination of the sample normal orientation agreed with the helicon measurements to within the accuracy of the x-ray photographs. The resolution of the helicon data was superior to the 0.5° x-ray determination.

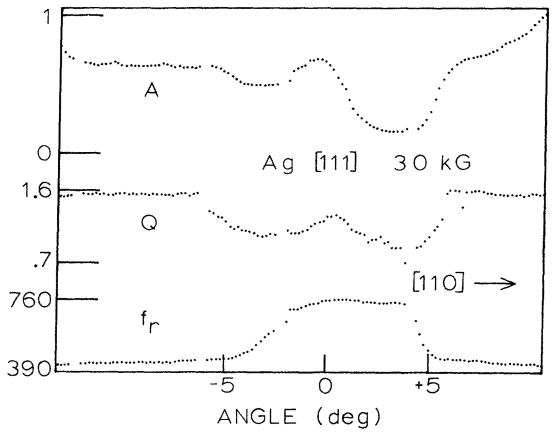

FIG. 2. Helicon parameters A, Q, and f_r as functions of crystallographic direction of field near the [111] axis in silver. The field direction rotated in the $(\bar{1}10)$ plane. The field magnitude B_0 was 30 kG. Each helicon resonance corresponds to one-half wavelength fitting inside the Ag sample plate of thickness 0.99 mm. The amplitude A is normalized; its scale is in arbitrary units. Q is a pure number which cannot be less than 0.5. The scale of the resonant frequency f_r is in Hz.

In Fig. 2 the sample was tipped so that B rotated in the $(\bar{1}10)$ plane; the [100] axis is off to the left in the figure. The resonant amplitude is shown on a normalized scale in the top curve. It exhibits a peak in the [111] direction with minima on both sides. This behavior is in agreement with earlier dc magnetoresistance measurements.[2] The behavior is due to the intersection of the Fermi surface with the Brillouin-zone edge in the [111] direction. The Brillouin-zone intersection gives rise to a region of extended cyclotron orbits when $\vec{B}_0$ is in a direction close to [111]. Only closed orbits exist when $\vec{B}_0$ is exactly parallel to [111]. In high fields the magnetoresistance is larger in regions of extended orbits then in regions of closed orbits.[1] The observed behavior of the amplitude reflects the fact that A is inversely proportional to the magnetoresistance. The Q of the resonance exhibits similar behavior and varies from 0.7 to 1.6. The difference in angular position of the maxima of

TABLE I. Silver sample characteristics.

Crystallographic direction of sample normal	Resistance ratio $\frac{R(300\text{ K})}{R(4.2\text{ K})}$ $(B_0=0)$	Sample thickness (mm)	Sample face shape	Smallest lateral dimension (mm)
[100]	850	1.12±2%	Circular	15
[110]	900	0.87±2.4%	Rectangular	13
[111]	830	0.99±3%	Rectangular	13
[211]	800	1.16±3.2%	Elliptical	16

A and Q is explained by a transverse even voltage. The resonant frequency varies from 390 to 760 Hz and exhibits a "mesa" whose width covers the region of extended cyclotron orbits.

Figure 3 shows results for the helicon parameters when $\vec{B}_0$ is in a direction close to [100]. A region of extended cyclotron orbits can be used to explain the results. The extended orbit regions on either side of the [100] axis are wider than the extended orbit regions on either side of the [111] axis. Q values varied from 0.5 to 1.7 and resonant frequencies from 280 to 380 Hz.

Figure 4 shows results from a [211] sample. All three parameters show a dip at [211]. It has been suggested that two perpendicular directions of open cyclotron orbits intersect at [211].[2] Q, in this case, varied from 0.5 to 1.4 and f_r varied from 240 to 360 Hz.

Figures 5–9 show the results of analysis of the helicon parameters to yield the resistivity tensor elements. In each case the field was 30 kG and experiments were done with both normal and reversed field to separate terms even and odd in field. The two upper curves in each figure show the parts of the off-diagonal element R_{xy} even and odd in magnetic field. These results were obtained using Onsager's relations

$$R_{ij}(B_0) = R_{ji}(-B_0) \tag{2}$$

and the formula

$$R_{xy} \propto A f_r / Q \ . \tag{3}$$

In each figure, both the even and odd terms are normalized with the same normalization constant.

The lower curves give results for the transverse

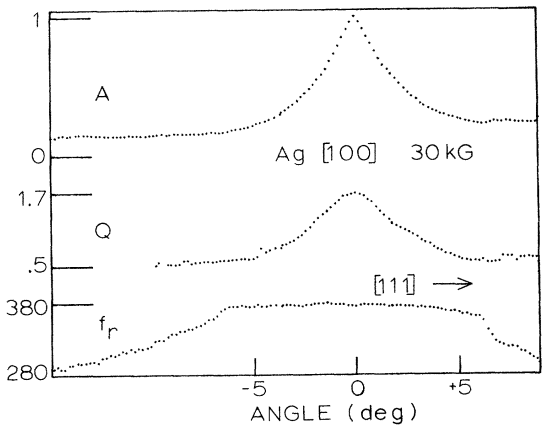

FIG. 3. Helicon parameters A, Q, and f_r as functions of field direction near [100]. The field direction rotated in the (0$\bar{1}$1) plane. B_0 was 30 kG. Sample thickness was 1.12 mm.

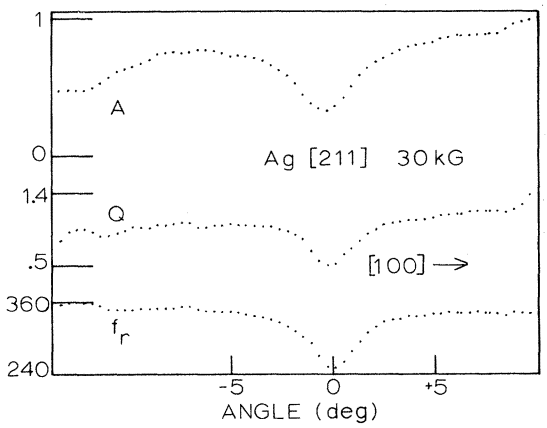

FIG. 4. Helicon parameters A, Q, and f_r for field directions near [211]. [111] is off to the left and [100] to the right. B_0 was 30 kG and sample thickness was 1.16 mm.

magnetoresistance, obtained from the formula

$$(R_{xx}+R_{yy}) = f_r/Q \ . \tag{4}$$

The magnetoresistance data are plotted as $\Delta R/R(0)$, where $R = \frac{1}{2}(R_{xx}+R_{yy})$ and $\Delta R = R(B_0) - R(0)$; $R(0)$ is the extrapolated value of R at zero field. ω_c is the cyclotron frequency of the majority carriers and τ is the average relaxation time; $\omega_c\tau = R_H(0)B_0/R(0)$, where $R_H(0)$ is the Hall coefficient at zero field.[2]

The error limits indicated on the figures are relative errors from point to point. A systematic error exists for the numerical values of the magnetoresistance R due to the uncertainty in the sample thickness. The inverse square of the thickness enters the expression for f_r [cf. Eq. (1c)]. Table I lists the uncertainties in sample thicknesses. Thus the value of R may be shifted by as much as twice the uncertainty given in Table I. The same uncertainty exists in the value of R at zero field $R(0)$. This error does not exist in the relative quantity $\Delta R/R(0)$.

Figure 5 shows the variation in R_{ij} elements near [100] as the direction of $\vec{B}_0$ rotated in the (0$\bar{1}$1) plane. In Fig. 6 the field direction rotated in the (1$\bar{1}$0) plane. The spurious discontinuity to the left of the [110] direction was caused by the interaction of the helicon signal with a mechanical resonance. Figure 7 shows data for the same [110] sample. In this case the field direction rotated in the the (00$\bar{1}$) plane. In Fig. 8 $\vec{B}_0$ rotated in the ($\bar{1}$10) plane. The data near the [211] direction in Fig. 9 were taken for variations of the field direction in the (01$\bar{1}$) plane.

Results for the tensor elements as functions of $\omega_c\tau$ for field directions along the major axes are

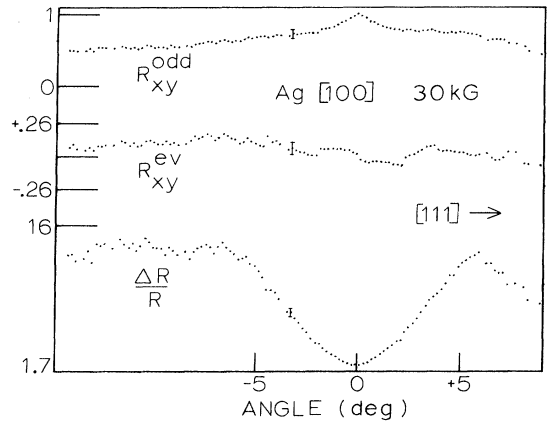

FIG. 5. Resistivity tensor elements for field directions near [100]. Upper two curves show terms in R_{xy} odd and even in field. Both curves are normalized with same constant. Top curve is the effective Hall coefficient as a function of angle; middle curve represents the transverse even term. Bottom curve shows transverse magnetoresistance. Fields used were ±30 kG.

shown in Figs. 10 and 11. Data at the lowest field ($\omega_c\tau \lesssim 2$) are suspect since the helicon signal is small and the Q of the resonance is close to 0.5. This can cause mixing between resonances corresponding to $\frac{1}{2}$ and $\frac{3}{2}$ helicon wavelengths inside the sample. A factor of $\vec{B}_0$ has been divided out of the curve for the part of R_{xy} odd in field. Assuming R_{xy} consists of only two terms

$$R_{xy} = R_H B_0 + C B_0^2,$$

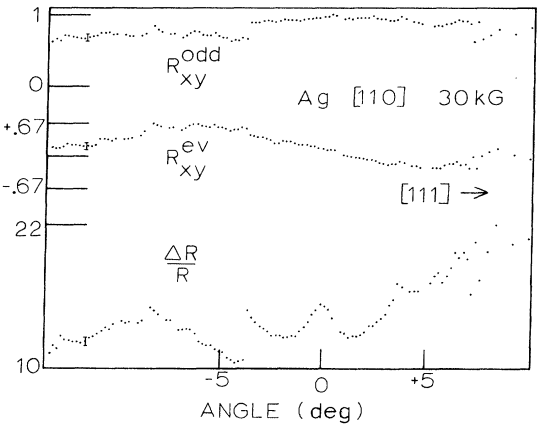

FIG. 6. Resistivity tensor elements for field directions near [110]. Discontinuity in magnetoresistance curve left of [110] is due to mechanical resonances. Fields were ±30 kG. Field direction rotated in the $(1\bar{1}0)$ plane.

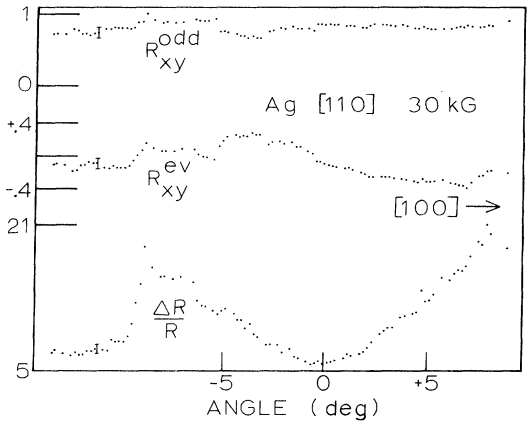

FIG. 7. Resistivity tensor elements for field directions near [110]. Fields were ±30 kG and rotated in the $(00\bar{1})$ plane.

this top curve gives the variation of the Hall coefficient R_H with magnetic field. A factor of B_0^2 has been taken out of the curve for the part of R_{xy} even in field. This second curve represents the transverse even voltage.[7]

The experimentally measured Q values may be used to determine an open-orbit carrier density, n_{op}, for open or extended orbit regions near a direction supporting only closed cyclotron orbits.[8] The effects of open-orbit carriers on helicon propagation can be understood assuming the Fermi surface is a sphere with intersecting cylinders.[9] Figure 12 shows the results around the [100], [111], and [110] axes. The ratio of electron density to hole density n_e/n_h was determined in each case with the field along the principal axis. The values of

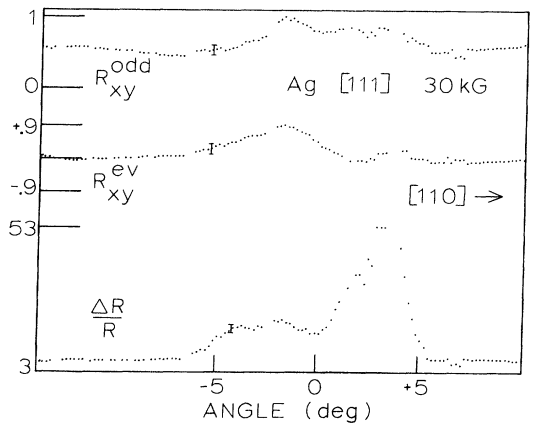

FIG. 8. Resistivity tensor elements for field directions near [111]. Fields were ±30 kG and rotated in the $(\bar{1}10)$ plane.

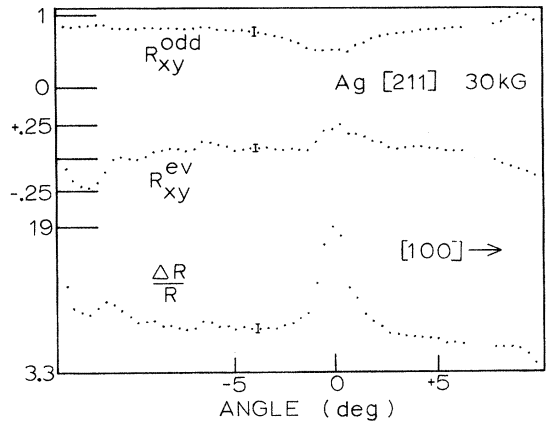

FIG. 9. Resistivity tensor elements for field directions near [211]. Fields were ±30 kG. [111] axis is off to left; [100] axis is to right.

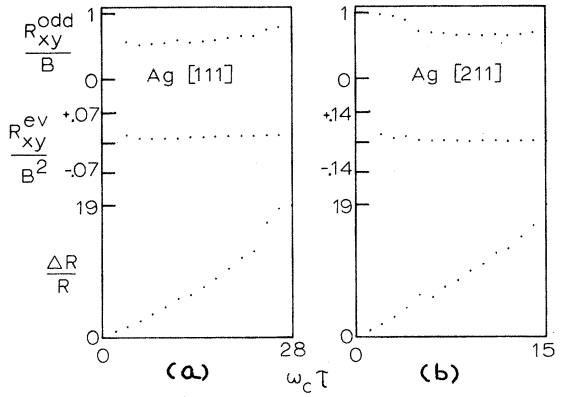

FIG. 11. Resistivity tensor elements as functions of $\omega_c\tau$. (a) Field direction parallel to [111]. (b) Field direction parallel to [211].

n_e/n_h were, 1.3, 1.3, and 1.2 for the [100], [110], and [111] directions, respectively. This ratio n_e/n_h is assumed to change slowly with orientation near the principal axis. The variation in n_{op} is pronounced.

IV. DISCUSSION

Knowledge of the variation of resistivity tensor elements, or electron transport properties, with direction in a crystal can be used as a check on Fermi-surface calculations. The presence of open or extended cyclotron orbits can be predicted from the shape of the calculated Fermi surface. Open orbits have marked effects on the R_{ij} elements and on the helicon parameters. The data we have presented indicate the angular widths of regions of open or extended orbits near the major axes. The relative magnitudes of the R_{ij} elements agree with existing data.[2,4]

Errors in the measurements are small. Errors in signal amplitude were generally less than 1% and errors in frequency were less than 0.5 Hz. The effects of finite sample size are not fully understood.[10] A more complete study of the helicon boundary-value problem remains to be done. In the present experiments a ratio of 15 for side length to thickness was assumed sufficient to be able to use results derived for an infinite flat plate. The exact effects of tipping on helicon propagation also are not known. For tipping up to 12° these effects

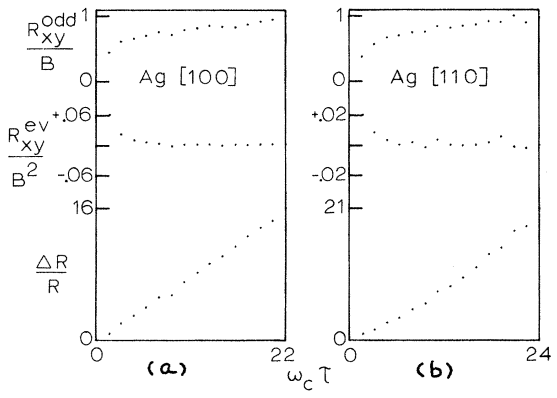

FIG. 10. Resistivity tensor elements as functions of $\omega_c\tau$. (a) Field direction parallel to [100]. (b) Field direction parallel to [110].

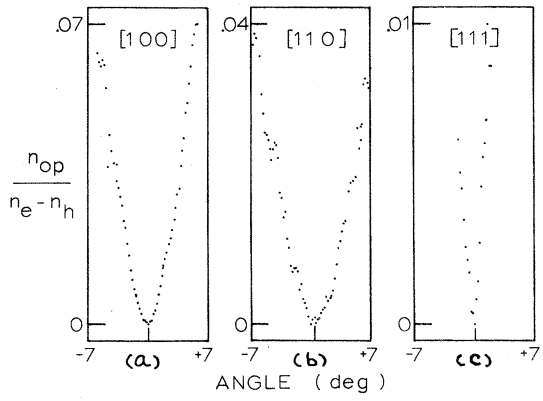

FIG. 12. Variation of open-orbit carrier density $n_{op}/(n_e - n_h)$ near the principal axes. Field was 30 kG. (a) For the [100] curve the field direction rotated as in Fig. 3. (b) For the [110] curve the field direction rotated as in Fig. 7. (c) For the [111] curve [100] is off to the left and [110] to the right.

are assumed small and have been neglected. For the data presented the major axis was always very close to the sample plate normal, so that much of the structure in the R_{ij} curves occurs for angles considerably less than 12°. A three-dimensional solution to the boundary-value problem would clarify the effects of tipping.

This paper presents the most complete study thus far of resistivity tensor elements using the helicon technique. The helicon method offers several advantages over conventional dc techniques. No leads need be attached to the sample, and the instrumentation is relatively inexpensive and straightforward to use. High resolution is possible in dc experiments as shown by the work of Klauder *et al.*[2] in copper. Comparable results are possible with the helicon method in metals of comparable purity. The helicon method has the disadvantage of requiring the solution of a boundary-value problem.

---

*Work supported in part by the Research Corporation, the U.S. Atomic Energy Commission [Contract No. AT (30-1)-4186] and the Samuel P. Hunt Foundation.

†Present address: Department of Engineering and Applied Science, Yale University, New Haven, Conn.

[1]I. M. Lifschitz, M. I. Azbel, and M. I. Kaganov, Zh. Eksperim. i Teor. Fiz. 31, 63 (1956) [Soviet Phys. JETP 4, 41 (1957)]; E. Fawcett, Advan. Phys. 13, 139 (1964).

[2]N. E. Alekseevskii and Yu. P. Gaidukov, Zh. Eksperim. i Teor. Fiz. 42, 69 (1962) [Soviet Phys. JETP 15, 49 (1962)]. For dc measurements of resistivity tensor elements in copper, see J. R. Klauder, W. A. Reed, G. F. Brennert, and J. E. Kunzler, Phys. Rev. 141, 592 (1966).

[3]R. G. Chambers and B. K. Jones, Proc. Roy. Soc. (London) A270, 417 (1962); P. A. Penz, J. Appl. Phys. 38, 4047 (1967).

[4]J. R. Merrill, Phys. Rev. 166, 716 (1968).

[5]M. T. Taylor, J. R. Merrill, and R. Bowers, Phys. Rev. 129, 2525 (1963).

[6]J. R. Merrill, M. T. Taylor, and J. M. Goodman, Phys. Rev. 131, 2499 (1963).

[7]J. R. Klauder and J. E. Kunzler, Phys. Rev. Letters 6, 179 (1961).

[8]S. W. Hui, J. Appl. Phys. 40, 3521 (1969).

[9]S. J. Buchsbaum and P. A. Wolff, Phys. Rev. Letters 15, 406 (1965).

[10]C. R. Legendy, Phys. Rev. 135, A1713 (1964).

PHYSICAL REVIEW B VOLUME 2, NUMBER 4 15 AUGUST 1970

Electronic Structure Effects in the Drude and Interband Absorption of Aluminum*

David Brust

Lawrence Radiation Laboratory, University of California, Livermore, California 94550

(Received 5 March 1970)

Using Ashcroft's potential, the interband and Drude absorption in aluminum have been calculated. Two large peaks occur in the interband part of $\epsilon_2(\omega)$ at 0.5 and 1.6 eV. In addition, the interband absorption continues as $\hbar\omega \to 0$. The optical effective mass is calculated with the result that $m_a^* = 1.45\, m_0$. Comparison with experiment is excellent. It is concluded that the optical spectrum of aluminum is completely understood in terms of the band structure. It is also pointed out that the optical peaks can be used to help determine the Fermi surface.

INTRODUCTION

Among the simple metals, aluminum is one of the most interesting from the point of view of electronic theory. This is due, in large part, to the success of the nearly free-electron (NFE) model in interpreting Fermi-surface experiments.[1,2] In this regard, Ashcroft[2] has shown that a simple two-parameter pseudopotential will account very nicely for the small departure from a completely free-electron picture.

Since the band structure of aluminum is expected to be well described by NFE model, one would hope to be in a position to account for its optical properties. The picture, however, is somewhat unclear. On the experimental side, optical response functions have been studied in the infrared and optical regimes by many investigators over the past few years.[3–12] Using the data available to them, Ehrenreich *et al.*[13] constructed the real and imaginary parts of the dielectric function. Using the infrared portion of the curves,